Atomistic simulations of distortion-limited high-speed dynamics of antiferromagnetic skyrmions

Elizaveta A. Tremsina and Geoffrey S. D. Beach

Phys. Rev. B **106**, L220402 — Published 8 December 2022

DOI: 10.1103/PhysRevB.106.L220402

Atomistic Simulations of Distortion-limited High-speed Dynamics of Antiferromagnetic Skyrmions

Elizaveta A. Tremsina

Department of Electrical Engineering and Computer Science, Massachusetts Institute of Technology, Cambridge, Massachusetts, 02139, USA and Department of Materials Science and Engineering, Massachusetts Institute of Technology, Cambridge, Massachusetts, 02139, USA

Geoffrey S.D. Beach

Department of Materials Science and Engineering, Massachusetts Institute of Technology, Cambridge, Massachusetts, 02139, USA

(Dated: November 25, 2022)

Abstract

In antiferromagnetic (AFM) materials, localized self-sustaining states called solitons, namely domain walls (DW) and skyrmions, can be efficiently driven by currents and achieve velocities of several kilometers per second. These solitons are massive particles and therefore cannot travel faster than a limiting velocity akin to the speed of light for the material. The specifics of these high velocity dynamics, in which solitons begin to display relativistic effects, have been well understood for the case of DWs (single-dimensional particles). Here, we perform an extensive and systematic atomistic study of both 1D and 2D soliton dynamics in chiral magnetic materials, both at and away from angular momentum compensation. For the first time, we develop an elastic restorative force model to explain the dynamic skyrmion deformations, supported by simulation data. We claim that these deformations arise from a local imbalance of gyrotropic forces. We also present a novel outlook on the role of skyrmion compactness in their deformation patterns, velocity limits, as well as the absence of behaviors similar to ones observed in relativistic DWs. We claim that limits on skyrmion compactness also impede their ability to reach the velocity regime where relativistic effects begin to occur in rapidly moving DWs, due to the critical skyrmion breakdown behavior. These res ults could prove to be significant to the field of spintronics, as well as the potential applications of skyrmions for novel logic and memory devices.

In the recent years, antiferromagnetic (AFM) materials have received much attention, due to the possibilities for spin-torque-driven rapid dynamics and potential use in storing bits of information. Of particular interest are AFM solitons, which are localised self-sustaining states with particle-like properties[1], namely domain walls (one-dimensional, parametrized by wall width Δ_{DW}) and skyrmions (two-dimensional, with radius R_{SK} and wall width Δ_{SK}), which can be efficiently driven by spin torques, such as spin-orbit (SOT) or spin-transfer (STT) Torques[2][3]. For the case of AFM DWs, numerous theoretical[4–8] and recently, experimental[9] studies have shown evidence of relativistic dynamics which fit into the framework of Lorentz invariance of magnons governed by the one-dimensional Sine-Gordon equation[10]. However, for the case of AFM skyrmions (AFMSk), although they have been studied as relativistic solitons[11, 12], there is a lack of full explanation of their high-velocity dynamics. In particular, conflicting conclusions have been made regarding the dynamic structural changes, the exact nature of these deformations, and most importantly,

whether they follow the same set of relativistic mechanisms as AFM DWs.

From the perspective of string theory, skyrmions are considered massive fermions in non-commutative space-time geometry[13–15], breaking Lorentz symmetry[16] and undergoing an elongation along the transverse dimension and a Lorentz-like contraction along the velocity direction[17]. From a fundamental perspective, solutions of the Sine-Gordon equation in ≥ 1 spatial dimensions were deemed different from the 1D case, in particular, the subset of slower-than-speed-of-light solutions cannot truly reach the speed of light[18]. Thus, the Lorentz invariance of AFMSks (2D solitons) is further put in question by their difference from single DWs (1D solitons). It also has not yet been shown that AFMSks can display relativistic effects such as emission of spin waves, as observed in travelling DWs. Nevertheless, previous simulation studies have observed significant elliptical deformations in travelling AFMSks[11, 12, 19, 20], which cannot be explained by the special relativistic length contraction phenomenon. It was also claimed that for the case of skyrmions in synthetic Antiferromagnets (SAF), the gyrotropic vector is responsible for the deformations and pulling apart of the SAFSk which consists of two coupled sublattice skyrmions[21]. Lastly, severe deformations, of a more irregular and asymmetric nature, have also been observed in ferromagnetic skyrmions (FMSk), with several explanations thereof[22–26]. However, the link between all of these skyrmion distortions and a physical explanation for their nature are yet to be uncovered.

Magnetic skyrmions are most often modeled with the 360° domain wall profile and parametrized by a radius R and wall width Δ_{SK}[27–30] (see Supplementary Material[31] for further discussion). Equilibrium AFMSk properties, i.e.stability conditions and physical dimensions (Δ_{SK}, R) are fully dictated by the continuous (atomistic) material parameters - exchange A (j_{ij}), anisotropy K (k_U) and the DMI D (d_{ij})[19, 30, 32, 33], more details in Supplementary Material[31]. The ratio $\frac{\Delta_{SK}}{R}$, we hereon call the compactness parameter. It determines how much of the skyrmion area is occupied by the inner region of nearly uniform magnetization, compared to the bounding wall: a small $\frac{\Delta_{SK}}{R}$ corresponds to a bubble skyrmion, while large $\frac{\Delta_{SK}}{R}$ gives a compact one. In this parametrization, the theoretically derived limit to maximum stable skyrmion compactness is $\frac{\Delta_{SK}}{R} \leq 1.14$ (corresponding to $\frac{R}{\Delta_{SK}} = \rho_{\min} = arcsinh(1) \approx 0.88$)[30] and will be referred to further.

The equilibrium dimensions of skyrmions have been previously derived by minimizing AFMSk energy, including contributions from 1).domain wall and 2).curvature energy terms,

given as[29, 34]

$$E_{SK}^{circ} = 2\pi R\sigma + \frac{4\pi A\Delta_{SK}}{R} \tag{1}$$

The DW energy density σ is defined in terms of material parameters as $\sigma \equiv 4\sqrt{AK} - \pi|D|$[34].

The dynamics of magnetic skyrmions is expressed by the generalized Thiele equation which is two-dimensional[19, 23, 25, 35]

$$\mathcal{M}\dot{\mathbf{v}}(t) + g\hat{z} \times \mathbf{v}(t) + \alpha\mathcal{D}\mathbf{v}(t) = \mathbf{F} \tag{2}$$

The first term corresponds to the skyrmion mass tensor, the second is the Magnus force, the third is the dissipative tensor and the right side represents the external force contribution. For the case of a circularly symmetric skyrmion (at rest), the dissipative tensor is diagonal and $\mathcal{D}_{xx} = \mathcal{D}_{yy} = \mathcal{D}_0$, where the dissipation constant $\mathcal{D}_0$ can be written as a function of equilibrium compactness[36]

$$\mathcal{D}_0 = \frac{1}{2}\left(\frac{R}{\Delta_{SK}} + \frac{\Delta_{SK}}{R}\right) \tag{3}$$

The Magnus force term acting on a magnetic skyrmion is $F_M = g\hat{z} \times v$, with gyrovector term g proportional to the topological charge Q[19, 37],

$$Q = \frac{1}{4\pi}\int dxdy\vec{m} \cdot \left(\frac{\partial}{\partial x}\vec{m} \times \frac{\partial}{\partial y}\vec{m}\right) \tag{4}$$

For a skyrmion in a fully compensated AFM material (Q=0), the total force acting on the skyrmion center of mass vanishes, and thus, it does not undergo deflection caused by the well-known Skyrmion Hall effect[20, 21, 38–40]. However, in a previous study of synthetic Antiferromagnetic (SAF) skyrmion tubes[21], it was shown that the gyrotropic force acting oppositely on the two SAF sublattices, causes 1).an elliptical elongation of the individual sublattice skyrmions, and 2).a vertical displacement and shear strain at the interface of the coupled FM layers. Thus, a potential local imbalance of gyrotropic forces acting on the two sublattices which could be at the core of the previously observed elliptical deformations in both SAF and AFM skyrmions and are considered in detail in this study.

It was analytically shown that, in the regime where soliton velocity is approximately linear with current, skyrmion velocity is always lower than that of a single DW under the same applied current density [30]. Velocity of solitons in an antiferromagnet is limited

by the maximum spin wave group velocity v_m, defined by the micromagnetic exchange constant A, atomic magnetic moment density μ_S, lattice parameter a and gyromagnetic ratio: γ as $v_m = \frac{\gamma A a^2}{2\mu_S}$[4, 6, 9]. Previous studies[4, 7, 9] have shown that AFM DWs display relativistic behavior due to the Lorentz invariance of magnons, leading to a contraction of the domain wall width and simultaneously a velocity saturation to v_m. This velocity-dependent contraction behavior aligns with the standard model of special relativity in which lengths of objects in a moving frame are scaled by the Lorentz factor $\frac{1}{\sqrt{1-\frac{v^2}{v_m^2}}}$[41]. Thus v_m acts as the 'speed of light' in the material system and the velocity of a moving DW can be written as a function of the width parameter as[4]

$$v_{DW} = v_m \sqrt{1 - \frac{\Delta^2}{\Delta_0^2}} \tag{5}$$

However, in a recent treatment of AFMSk dynamics, it was claimed that they cannot be accelerated to a constant terminal velocity arbitrarily close to v_m and are bounded by a critical velocity value v_c[12]. This limit was defined analytically as a fraction of v_m via an expression that involves all three material parameters[12].

$$v_c = \sqrt{1 - \frac{\pi^2 D^2}{16AK}} v_m \tag{6}$$

However, this treatment of the skyrmion as a massive particle and solitary wave[12] with relativistic energy modified by the presence of DMI in the system, leads to a defined critical behavior but does not provide an intuitive explanation of the nature of these deformations.

In the following, we present numerical results from atomistic simulations of spin-orbit torque driven motion of single DWs and AFMSks, performed in VAMPIRE[42]. Unlike certain previous modelling studies of AFM solitons, here we systematically sweep over a wide range of material parameters, uncovering important fundamental relationships between dynamics and equilibrium structural parameters. These modelling results allow us to develop an explanation of skyrmion distortions, based on the imbalance of the gyrotropic forces. We also examine the high-velocity limits of both skyrmions and DWs in AFM materials and provide a discussion of the possibility of attaining relativistic behaviors in AFMSk. Lastly, we explore the similarities between antiferromagnetic and ferromagnetic skyrmion distortions by examining ferrimagnetic skyrmion dynamics at high speeds, and conclude that the nature of deformation-limited high-speed behavior appears to be universal across these classes of

materials.

Atomistic simualtions are performed in the open-source VAMPIRE[42] package, with slight custom code modifications to include the initialization of magnetization textures such as isolated skyrmions or DWs. See Supplementary Material[31] for further details about the atomistic model used in this study. We set up a single-atomic-layer magnetic racetrack-like region with periodic boundary conditions (PBC) along the longer dimension (x-axis). The y-dimension is chosen to be 70nm, much wider than all modeled equilibrium skyrmion radii. The material has perpendicular magnetic anisotropy (PMA) along the z-axis. The damping constant $\alpha = 0.001$ and the lattice constant $a = 4\mathring{A}$. Upon initialization of the magnetization profiles using the functions for skyrmions and DWs, we run an equilibration procedure to retrieve the soliton state and dimensions. Dynamics are made possible through a Slonczewski-like (damping-like) torque $B_{D,i}$ which is specified per magnetic lattice moment i and calculated as $B_{D,i} = \frac{\hbar\theta}{\mu_s q_e t_z} j_{HM}$[4]. Here the μ_s is the respective magnetic moment density, $\theta = 0.1$ is the Spin Hall angle, while $t_z = 1nm$ is the modeled thickness of the film. j_{HM} is the modeled current density flowing in the x-direction in the adjacent heavy-metal layer which supplies the spin-orbit torque acting on the magnetic film and allowing for the motion of solitonic particles. The direction of spin polarization here is along $-\hat{y}$, thus the torque on magnetic spin at site i is proportional to $B_{D,i}(\mathbf{S}_i \times (\mathbf{S}_i \times \hat{y}))$, causing the skyrmion to move from left to right.

First, we show a side-by-side comparison of current-driven dynamics for single DWs and AFMSks in the same material. The particular atomistic material parameters were chosen similar to [4]: Heisenberg exchange $j_{ij} = 2.56 \times 10^{-21} J$, perpendicular anisotropy $k_U = 8 \times 10^{-24} J$, magnetic moment per atom $\mu_S = 3.45\mu_B$ and DMI $d_{ij} = 6 \times 10^{-23} J$, for a lattice constant of $a = 4$Å, and various current densities in the range $j \in (2-60) \times 10^{11}$A/m^2.

Fig.1a shows the intermediate two-dimensional snapshots of travelling AFMSks accelerated from rest. We observe that the skyrmion becomes approximately elliptical in shape, as seen previously[11, 12, 38]. The longer axis of the ellipse which we call R_y, is oriented perpendicular to the direction of motion. Fig.1b-c demonstrate the differences in terminal velocities and dynamically changing dimensions of AFMSks and DWs, as a function of applied current density. Both v_c and v_m for the material are marked in Fig.1b. As seen previously[12], we show the increase in both semi-major (R_y) and semi-minor axial dimensions (R_x), as compared to equilibrium radius R_0 of the AFMSk. One can differentiate

between two regimes of AFMSk dynamics (stable and unstable), which are separated by the critical velocity limit v_c. We show that for certain values of j (green points in Fig.1b and Fig.1c), AFMSk achieves a stable terminal velocity and size, here at $j \leq 22 \times 10^{11}\text{A/cm}^2$. However, accelerating the AFMSk to a faster speed via larger currents causes a continuous stretching of the skyrmion along the transverse direction, until it reaches the edges of the racetrack and fully deforms into a pair of single DWs. In other words, a stable skyrmion structure cannot be accelerated beyond this velocity limit, and it will elongate indefinitely, until reaching the width of the racetrack and becoming simply a pair of straight DWs (see case 4 in Fig.1b and Supp Video 1).We have verified that the finite track width does not significantly affect the velocity threshold at which runaway expansion occurs by performing a set of simulations with track width varying between X and Y. As claimed by [12], these deformations and eventual structure breakdown constitute the limit to how fast an AFMSk of a certain material can travel, in other words, represent valid solutions of the equation of motion for a solitary wave.

Conversely, for a single DW (blue squares in Fig.1b-c), our results confirm the standard relativistic behavior where the velocity saturates to v_m. The analytical fit (blue solid line) is taken from Eq.5 using the extracted contracting width Δ_{DW} from Fig.1c and agrees well with the simulation results in Fig.1b. We also point out the approximately linear AFMSk velocity dependence on current density (green points in Fig.1b), even despite the significant change in AFMSk dimensions and structure, as compared to the DW sublinear velocity function. Evidently, for the cases of destabilized AFMSks, the resulting DW pair displays the same velocity-current dependence as a single DW, as seen in the green rectangles in Fig.1a, where the blue and green points coincide.

We also discuss the reversibility of deformation and runaway expansion, not studied previously, with results shown in Fig.1d-e. Here we focus on a particular current density j which destabilizes the skyrmion and distorts it into a pair of DWs in a time $\tau_{dist} = 340$ps. Here we apply a current pulse starting at time=0ps, and then set $j_{HM} = 0$ at several times $\tau < \tau_{dist}$, and record the dynamic quantities at each time step. The skyrmion expands in size as it is being accelerated approximately to its critical velocity, and removing the current pulse before $\tau_c = 300$ allows for a full return to equilibrium state, after a deceleration. For the case when $\tau = \tau_c$, we observe an initial shrinking but then a full collapse of the skyrmion structure. Thus, the deformations can be fully reversed only before a certain

threshold expansion time τ_c which is less than τ_{dist}, the time it takes to fully reach the edges of the racetrack. As seen in panel (e), barring minor oscillations in R_y during the shrinking phase (current OFF), the extracted radius R_y follows the same relationship with v/v_m as during the expansion phase (current ON). We claim this result allows one to view skyrmion deformation in the context of velocity and energy dissipation, instead of the specific torques acting on it to drive the motion.

We next present a novel outlook on critical velocity v_c and dynamic deformation, by claiming they are actually strongly connected to equilibrium AFMSk structure. For this, we choose a particular set of material parameters to produce stable AFMSks of different compactness values, ranging from 0.25 to 1.135. Fig.2 shows the dynamics of AFMSks of various compactness values (ranging from perfectly compact in the top row to more bubble-like in the bottom panel). The two(one)-dimensional equilibrium AFMSk profiles are shown in panel a(b). Panel (c) clearly demonstrates the runaway nature of transverse AFMSk expansion, in the plot for the change in R_y as a function of fractional velocity v/v_m. The red dashed line marks the particular value of v_c for each AFMSk. As compactness decreases, so does the ability of the AFMSk to attain higher fractional velocities, and this behavior aligns with the earlier onset of the runaway expansion.

To generalize this concept further, we perform sets of simulations for AFMSks corresponding to a large subspace of material parameters $\Theta = \{A, D, K\}$, thus varying equilibrium dimensions, as well as the velocity limits v_m and v_c. More details on the specific parameter choice are found in the Supplementary Material[31]. As discussed above, for the 1D case (single DWs), relative changes in width $\Delta_{DW}(v)/\Delta_{DW}(0)$ can be always directly mapped to the velocity relative to v_m, which is evident from Eq.5. However, as seen in Fig.3a, there is no clear relationship between the scaled AFMSk deformation and the fractional velocity with respect to v_m. Instead, our results in Fig.3b show that no matter the equilibrium AFMSk dimensions, $\frac{R_y}{R_0}$ values do follow a specific functional relationship with the velocity scaled by $v_c(\Theta)$. We also note that although it was argued[11, 17] that AFMSk radii change as a function of $\frac{v}{v_m}$, only a single set of material parameters was considered there, corresponding to a compact skyrmion. Instead here, we find that the dominant transverse deformation effect does not parallel the Lorentz contraction of coordinate space in the direction of motion as in single DWs, but that there is a change in the structural properties of the soliton itself, as it is stretched out perpendicular to motion direction.

Furthermore, we reveal the fundamental nature of the critical velocity v_c, and the significant role it plays in AFMSk dynamics and structural changes. To summarize, although the exact function f is still to be determined, simulation results demonstrate that for the parameter set Θ, the following universal relation holds for $v_c(\Theta)$ but not for $v_m(\Theta)$.

$$\frac{R_y}{R_0}(\Theta, v) = f\left(\frac{v}{v_c(\Theta)}\right) \tag{7}$$

We return to the concept of AFMSk compactness and specifically show how it can be directly related to the critical dynamics. One existing theoretical prediction of AFMSk dimensions from input material parameters was derived as[29]:

$$R^W = \frac{\pi D/4K}{\sqrt{1-(\frac{\pi^2 D^2}{16AK})}}, \quad \Delta_{SK}^W = \frac{\pi D}{4K} \tag{8}$$

$$\frac{\Delta_{SK}^W}{R^W} = \left(1 - \frac{\pi^2 D^2}{16AK}\right)^{\frac{1}{2}} \tag{9}$$

Comparing the theoretical expressions Eq.9 and Eq.6, one can write the normalized critical deformation velocity as $\frac{v_c}{v_m} = \frac{\Delta_{SK}^W}{R^W} \approx \frac{\Delta_{SK}}{R}$.

To test this hypothesis, we perform atomistic simulations over a wide parameter range, shown in Fig.3c. The horizontal axis shows the equilibrium skyrmion compactness value which is extracted after stabilization of the initialized skyrmion magnetization profile. To estimate v_c, we performed a set of simulations with varying current density to identify the boundary between stable and unstable dynamics. We classified the skyrmion as dynamically stable if the transverse dimension asymptotically approached a fixed value less than the track width during the simulation time, and unstable if the rate of change of the transverse dimension increased continuously until it reached the track width. The value of v_c reported in Fig.3c corresponds to the maximum velocity at which stable motion was observed. The error bar is estimated as the product of the slope dv/dj at the stability boundary times the uncertainty of the critical current. The latter was set by the current density increments used in the set of simulations. It is clear from the results that increasing compactness leads to a higher critical deformation velocity limit, allowing the skyrmions to travel closer to the magimium group velocity v_m. We note that the expressions in Eq.9 only hold true for the regime where $R >> \Delta_{SK}$[29] and therefore, do not apply as well for compact skyrmions (high values of $\frac{\Delta_{SK}}{R}$). We find that the relationship between the two plotted variables is not strictly linear, especially as $\frac{\Delta_{SK}}{R}$ increases (compact AFMSk).

To test the robustness of this relationship between compactness and normalized critical velocity, this process was repeated for several highly compact AFMSk, varying the material parameters in such a way as to maintain the ratio $\frac{D^2}{AK}$ constant, as shown in Fig.3d. All the modelled AFMSks have equal theoretical values of v_c/v_m, however, the actual physical dimensions R and Δ_{SK} are simultaneously scaled. However, despite this scaling of the skyrmion sizes, we see little deviation in the resulting normalized v_c, as shown in the red. This again underlines the universal importance of compactness over actual physical AFMSk dimensions, for understanding dynamic deformation and critical skyrmion behavior.

In the following, using numerical simulation data, we consider the local gyrotropic and elastic restoring forces acting on the sublattices of AFMSk. We argue that their competition leads to skyrmion deformations which can be dynamically stable or unstable. For that, we return to the Thiele equation 2, specifically the gyrotropic force term which includes the integral defined in Eq.4. The total integral vanishes for an AFMSk, however, here we show that the integrand function varies along the skyrmion perimeter. This gives rise to a spatially varying gyrotropic force term, involving the sublattice magnetic moment μ_S and gyromagnetic ratio γ [21, 30, 39]

$$f_G(\vec{r}) \propto \frac{\mu_S}{\gamma} g(\vec{r}) \left(\hat{z} \times \vec{v} \right) \propto g(\vec{r}) \hat{y} \tag{10}$$

$g(\vec{r})$ defines the spatially varying integrand function. For each of the material types $\eta \in (A, B)$ (corresponding to the two sublattices in the crystal AFM), we can extract the following quantity from our numerically simulated AFMSk magnetization profiles:

$$g(\vec{r}) = g^A(\vec{r}) + g^B(\vec{r}) \tag{11}$$

$$g^\eta(\vec{r}) = \vec{m}^\eta \cdot \left(\frac{\partial}{\partial x} \vec{m}^\eta \times \frac{\partial}{\partial y} \vec{m}^\eta \right) \tag{12}$$

Thus, a positive(negative) value of the g-factor corresponds to a local force pointing in the +(-) y-direction or up(down) in the given coordinate system. Fig.4 panel (a) shows the numerically calculated spatial distributions of the force as defined in Eq.10 for three AFMSks of various compactness values, displayed in arbitrary units. For each case, the left-most panel shows the equilibrium cases, where the net force summed over the perimeter is zero, while a top-bottom asymmetry emerges when the skyrmion is in motion.

We also extract the difference in forces acting on the top and bottom half-skyrmions, plotted in Fig.4(b). This quantity is zero at rest and increases linearly with velocity, as shown for the same three AFMSk cases. Thus, the magnitude of the resulting net gyrotropic force term, acting locally on the top/bottom skyrmion points, can be written as a square of the velocity in terms of a proportionality constant α_g.

$$F_G = \alpha_g \frac{\mu_S}{\gamma} v^2 \tag{13}$$

Here we assume that in dynamic equilibrium, (stretched AFMSk is travelling with a constant terminal velocity) the local gyrotropic force derived above is balanced by a restoring force acting to preserve the skyrmion structure, given by the change in its energy (here again in micromagnetic units) caused by a small increase in the radius R_y

$$\frac{dE_{SK}}{dR_y}(R_y) = F_G(v) \tag{14}$$

To produce the right-hand side of Eq.14, we modify the equilibrium skyrmion energy (Eq. 1), to account for elliptical deformations, making use of some approximations. It is assumed that $R_x \approx R_0$, or the parallel elliptical axis is approximately equal to the equilibrium value. Then, the first term in Eq.1 becomes proportional to the elliptical perimeter, given as

$$E_{DW} = \sigma P \approx \sigma\pi\sqrt{2(R_0^2 + R_y^2)} \tag{15}$$

The second energy term is proportional to the curvature

$$E_C = 2A\Delta_{SK} \int_0^{2\pi} \kappa(\phi) d\phi \tag{16}$$

The local curvature of an ellipse is defined as a function of polar angle ϕ as

$$\kappa(\phi) = \frac{R_0 R_y}{(R_0^2 \sin^2\phi + R_y^2 \cos^2\phi)^{3/2}}$$

However, the above has no analytical solution, thus we can either 1).apply a numerical calculation or 2).use an approximate form. For the latter, we approximate the total curvature as an average of the maximum and minimum values of $\kappa(\phi)$ as

$$\kappa \approx \frac{1}{2}\left(\frac{R_y}{R_0^2} + \frac{R_0}{R_y^2}\right) \tag{17}$$

With this curvature expression, the energy can be written as

$$E_C = 2\pi A\Delta\left(\frac{R_0}{R_y^2} + \frac{R_y}{R_0^2}\right) \tag{18}$$

Then, the total skyrmion energy and derivatives are

$$E_{SK} = \pi\sqrt{2(R_0^2 + R_y^2)} + 2\pi A\Delta\left(\frac{R_0}{R_y^2} + \frac{R_y}{R_0^2}\right) \tag{19}$$

$$\frac{dE_{SK}}{dR_y} = \pi\sigma\frac{R_y/R_0}{\sqrt{2 + 2R_y^2/R_0^2}} - 2\pi A\Delta\frac{2R_0}{R_y^3} + \frac{2\pi A\Delta}{R_0^2} = \pi\sigma\left(\frac{R_y/R_0}{\sqrt{2 + 2R_y^2/R_0^2}} - \frac{R_0^3}{R_y^3} + \frac{1}{2}\right) \tag{20}$$

The last expression was written using the equilibrium radius which minimizes Eq.1. To verify the model, we compare it to the numerically extracted data from the atomistic simulations, plotted in Fig4(c). The extracted pairs of numerical data (R_y and velocity) are shown using square points and compared against the two semi-analytical curves. Those are computed as follows. First, we use the numerical values of R_y, integrate over the angle ϕ as in Eq.16 to calculate the left-hand side of Eq.14 and differentiate numerically with respect to R_y (dashed line), then solving for v. Second, we instead use the numerical values of v, calculate the right-hand side of Eq.14 and solve for R_y assuming Eq.20 (solid line). Both expressions show good agreement with the numerical data. Thus, we provide a quantitative and visual proof of the local imbalance of forces acting to pull apart the skyrmion as it travels in a straight line. The self-consistency with our data suggests that the proposed model can be used to explain the deformation process, which has not been well understood previously.

The above simulation results for AFM skyrmion dynamics clearly demonstrate a critical underlying connection between compactness, deformation and velocity limits. Additionally, significant efforts have been made to understand in particular the dynamic deformations of ferromagnetic (FM) skyrmions[23, 24, 26, 43]. Here, by considering dynamics of ferrimagnetic skyrmions (FiMSks), we argue that skyrmion deformations are actually of similar nature in all of these material classes. As was previously shown with Monte Carlo simulations of FMsk motion, the observed dynamic deformations cause a change in the dissipative tensor[23], in particular an increase of the transverse effective mass component. This increase in effective mass along the y-axis was also explored for the AFMSk case by [12], and therefore can be considered common for magnetic skyrmions broadly.

Based on analytical expressions[44], a skyrmion with a nonzero net angular momentum ($\delta S \neq 0$) when driven by spin-torques, travels at an angle to the current direction, known as the skyrmion Hall Angle θ_{SK}, which scales depending on equilibrium skyrmion dimensions via the aforementioned dissipative constant $\mathcal{D}_0$ (see Eq.3) as well as damping constant α:

$$\theta_{SK} = \tan^{-1}\left(\frac{v_y}{v_x}\right) = \tan^{-1}\left(\frac{1}{\alpha_{eff}\mathcal{D}_0}\right) \tag{21}$$

The effective damping constant for a ferrimagnetic material can be expressed as the ratio of total spin to net angular momentum as $\alpha_{eff} = \alpha\frac{\sum|M_{S,i}|}{|\sum M_{S,i}|} = \alpha\left(\frac{\delta S}{S_{net}}\right)^{-1}$[9]. Thus, expression 21 can simply be rewritten as

$$\theta_{SK} = \tan^{-1}\left(\frac{2}{\alpha}\frac{\delta S}{S_{net}}\frac{1}{\left(\frac{R}{\Delta_{SK}} + \frac{\Delta_{SK}}{R}\right)}\right) \tag{22}$$

To study the effects of nonzero angular momentum on skyrmion deformation and critical velocity, we perform a set of dynamics simulations over a range of $\delta_S = S_1 - S_2$, ($S_i = \frac{\mu_i}{\gamma_i}$), symmetrically varying individual sublattice magnetic moments μ_i, while keeping the total moment $|\mu_1| + |\mu_2|$ and the individual gyromagnetic ratios γ_i constant (constant S_{net}). Fig.5 panels a-h correspond to the dynamics of FiMSks for a particular combination of A, K and D resulting in $\frac{\Delta_{SK}}{R} \approx 0.635$. Note that equilibrium FiMSk dimensions are not affected by the presence of net angular momentum, since no external magnetic field is present[33]. Our simulation data agree well with the analytical expression in panel a.

Starting with a perfectly AFM case, with a larger net momentum, we observe not only a larger deflection (increasing θ_{Hall}) but also a gradual decrease in the critical velocity, or the maximum velocity attained by the travelling skyrmion. This is evident from Fig.5h, where we plot the extracted v_c scaled by the maximum magnon group velocity that can be achieved in a material with this particular set of A, K, D and S_{net}. We also consider a few additional subsets of material parameters, resulting in FiMSks of various compactness values, and extract the critical velocity v_c for each (Fig.5i). Here we see again the high correlation between equilibrium compactness and critical velocity, and a steep drop-off as a function of net angular momentum.

Using our simulation results for critical velocity over a range of angular momenta, combined with the theoretical framework of transverse dissipation[23], we can argue that the dynamic deformations of AFMSk, FiMSk and FMSk are all related and dictated by their topological nature. Evidently though, AFMSks are the fastest travelling two-dimensional solitons that can achieve speeds closest to the range of relativistic DW velocities, because moving away from angular momentum compensation causes a decrease in v_c. Although not considered here, we note that effects of compensation on DW motion have been considered previously[45], concluding that FiM DWs have a limiting velocity, thus bridging the gap between AFM Dws, (limited only by v_m) and FM DWs (which undergo the Walker breakdown). Further inquiry into the analytical modeling of v_c as a function of δ_S for FiMSks is needed, to support our numerical findings.

Finally, we discuss the possibility of skyrmions showing relativistic behavior in the form of Spin Wave emission (SWE), as observed previously in single DWs[4, 6]. This emission away from the DW velocity direction is said to be the energy dissipation mechanism which accompanies DW velocity saturation at high increasing current density. Tatara et al.[5] presented a detailed theoretical analysis of magnon emission from a relativistic travelling AFM DW, claiming a significant enhancement of the magnon response functions for fast moving DWs. The exact velocity at which one begins to see SWE was shown to depend on several factors, including the magnon mode energy gap, dispersion function and transferred momentum from the DW to the magnon, however, was shown to happen as an example, at $v_{DW} \sim 0.8 v_m$[5].

Recently, the onset of SWE as a function of applied current density was studied for several values of exchange constant A, but not in the context of relative velocities[6]. Here instead, we perform a series of single DW simulations for the same set of parameters as in Fig.3, with the intention of comparing the onset of SWE to the physically allowed velocity range of travelling skyrmions. As a general metric for the SWE onset in DWs, we use the maximum spatial wavevector, extracted by taking the Fourier transform of the M_y profile behind the single DW, plotted against the fractional velocities v/v_m, noting that v_m here depends on the material parameters chosen. As shown in Fig.6, this is a valid metric, since a pronounced increase in the wavevector is seen as the DW reaches the relativistic regime, displaying the high frequency oscillations. This occurs just after $0.8 v_m$, and all curves follow the same hockey-shaped relationship, despite the differences in equilibrium DW widths. Thus, our

results for the single DW dynamics support the theoretical discussion in [5] which highlights the significance of proximity to v_m for the emergence of relativistic effects in the form of SWE.

Now, returning to skyrmions (here we focus exclusively on AFMSks due to their higher critical velocity than FiMSks), we have shown that the maximum compactness itself limits the maximum value $v_c^{\max} \approx 0.844 v_m$. As shown in Fig.6, the most compact AFMSk case has a critical velocity which very closely matches the increase in the wavevector and onset of SWEs in DWs. Although further rigorous theoretical explanation is needed for these purely numerical findings, our results lead us to argue that there may be an underlying connection between the mechanisms which govern the onset of SWE in AFM DWs, as well as the asymptotic velocity limit for a stable travelling AFMSk.

In this work, we uncover important underlying trends in dynamics of skyrmions and domain walls over a wide range of material parameters. In a side-by-side comparison of soliton dynamics, we demonstrate the unique critical nature of AFMSk dynamics, as compared to DWs. In a systematic parameter sweep, informed by previous theoretical arguments of skyrmion energetics and motion, we show the unversality of v_c for skyrmions at large (including AFM, as well as FiM) and its dependence on equilibrium structure. We emphasize the role of compactness over individual skyrmion dimensions and show how it also limits the ability of skyrmions to reach relativistic velocity effects, as observed in DWs. Lastly, we provide a semi-analytical model, supported by out numerical calculations, to explain the deformation process in an intuitive way, which has not been done previously, to the authors' knowledge.

ACKNOWLEDGMENTS

This work was supported in part by the DARPA TEE program and by SMART, one of seven centers of nCORE, a Semiconductor Research Corporation program, sponsored by National Institute of Standards and Technology (NIST). The authors would also like to thank the reviewers for their time and effort in reviewing the manuscript, especially the valuable comments and suggestions which led to the development of the gyrotropic tensor

explanation and model for AFMSk distortions.

---

[1] A. N. Bogdanovand C. Panagopoulos, The emergence of magnetic skyrmions, Physics Today **73**, 44 (2020).

[2] V. Baltz, A. Manchon, M. Tsoi, T. Moriyama, T. Ono, and Y. Tserkovnyak, Antiferromagnetic spintronics, Rev. Mod. Physics **90**, 015005 (2018).

[3] K. Koumpouras, A. Bergman, O. Eriksson, and D. Yudin, A spin dynamics approach to solitonics, Scientific Reports **6** (2016).

[4] T. Shiino, S.-H. Oh, P. M. Haney, S.-W. Lee, G. Go, B.-G. Park, and K.-J. Lee, Antiferromagnetic domain wall motion driven by spin-orbit torques, Phys Rev Lett **117**, 87203 (2016).

[5] G. Tatara, C. A. Akosa, and R. M. Otxoa de Zuazola, Magnon pair emission from a relativistic domain wall in antiferromagnets, Physical Review Research **2**, 043226 (2020).

[6] Z. Zhu, K. Cai, J. Deng, V. Pavan, K. Miriyala, H. Yang, X. Fong, and G. Liang, Electrical Generation and Detection of Terahertz Signal Based on Spin-Wave Emission From Ferrimagnets, Physical Review Applied **10**, 34040 (2020).

[7] H. Yang, H. Y. Yuan, M. Yan, H. W. Zhang, and P. Yan, Atomic antiferromagnetic domain wall propagation beyond the relativistic limit, Physical Review B **100**, 24407 (2019).

[8] S. H. Ohand K. J. Lee, Ferrimagnetic domain wall motion induced by damping-like spin-orbit torque, Journal of Magnetics **23**, 196 (2018).

[9] L. Caretta, S. H. Oh, T. Fakhrul, D. K. Lee, B. H. Lee, S. K. Kim, C. A. Ross, K. J. Lee, and G. S. Beach, Relativistic kinematics of a magnetic soliton, Science **370**, 1438 (2020).

[10] J. F. Currie, Aspects of exact dynamics for general solutions of the sine-Gordon equation with applications to domain walls, Physical Review A **16**, 1692 (1977).

[11] A. Salimath, F. Zhuo, R. Tomasello, G. Finocchio, and A. Manchon, Controlling the deformation of antiferromagnetic skyrmions in the high-velocity regime, Physical Review B **101**, 24429 (2020).

[12] S. Komineasand N. Papanicolaou, Traveling skyrmions in chiral antiferromagnets, SciPost Physics **8**, 086 (2020).

[13] Pratul Bandyopadhyay, Noncommutative Geometry: Physical Perspective, in *Geometry, Topology and Quantum Field Theory* (Springer Netherlands, Dordrecht, 2003) Chap. 6, pp.

165–203.

[14] V. Pasquier, Skyrmions in the quantum Hall effect and noncommutative solitons, Physics Letters B **490**, 258 (2000).

[15] B.-H. Lee, K. Moon, and C. Rim, Noncommutative field theory description of quantum Hall skyrmions, Physical Review D **64**, 10.1103/PhysRevD.64.085014 (2001).

[16] S. M. Carroll, J. A. Harvey, V. A. Kostelecký, C. D. Lane, and T. Okamoto, Noncommutative Field Theory and Lorentz Violation, Physical Review Letters **87**, 141601 (2001).

[17] D. Bakand K. Lee, Elongation of moving noncommutative solitons, Physics Letters, Section B: Nuclear, Elementary Particle and High-Energy Physics **495**, 231 (2000).

[18] Y. Zarmi, Sine-Gordon Equation in (1 +2) and (1+3) dimensions: Existence and Classification of Traveling-Wave Solutions, PLoS ONE **10**, 124306 (2015).

[19] J. Barkerand O. A. Tretiakov, Static and Dynamical Properties of Antiferromagnetic Skyrmions in the Presence of Applied Current and Temperature, Physical Review Letters **116**, 147203 (2016).

[20] C. Jin, C. Song, J. Wang, and Q. Liu, Dynamics of antiferromagnetic skyrmion driven by the spin Hall effect, Applied Physics Letters **109**, 182404 (2016).

[21] J. Xia, X. Zhang, K.-Y. Mak, M. Ezawa, O. A. Tretiakov, Y. Zhou, G. Zhao, and X. Liu, Current-induced dynamics of skyrmion tubes in synthetic antiferromagnetic multilayers, Physical Review B **103**, 174408 (2021).

[22] K. Litzius, I. Lemesh, B. Krüger, P. Bassirian, L. Caretta, K. Richter, F. Büttner, K. Sato, O. A. Tretiakov, J. Förster, R. M. Reeve, M. Weigand, I. Bykova, H. Stoll, G. Schütz, G. S. Beach, and M. Klaüi, Skyrmion Hall effect revealed by direct time-resolved X-ray microscopy, Nature Physics **13**, 170 (2017).

[23] A. W. Teixeira, S. Castillo-Sepúlveda, L. G. Rizzi, A. S. Nunez, R. E. Troncoso, D. Altbir, J. M. Fonseca, and V. L. Carvalho-Santos, Motion-induced inertial effects and topological phase transitions in skyrmion transport, Journal of Physics: Condensed Matter **33**, 265403 (2020).

[24] L. Liu, O. J. Lee, T. J. Gudmundsen, D. C. Ralph, and R. A. Buhrman, Current-Induced Switching of Perpendicularly Magnetized Magnetic Layers Using Spin Torque from the Spin Hall Effect, Physical Review Letters **109**, 096602 (2012).

[25] R. E. Troncosoand A. S. Nunez, Brownian motion of massive skyrmions in magnetic thin films,

Annals of Physics **351**, 850 (2014).

[26] J. Masell, D. R. Rodrigues, B. F. Mckeever, and K. Everschor-Sitte, Spin-transfer torque driven motion, deformation, and instabilities of magnetic skyrmions at high currents, PHYSICAL REVIEW B **101**, 214428 (2020).

[27] O. Boulle, J. Vogel, H. Yang, S. Pizzini, D. De Souza Chaves, A. Locatelli, T. O. Menteş, A. Sala, L. D. Buda-Prejbeanu, O. Klein, M. Belmeguenai, Y. Roussigné, A. Stashkevich, S. Mourad Chérif, L. Aballe, M. Foerster, M. Chshiev, S. Auffret, I. M. Miron, and G. Gaudin, Room-temperature chiral magnetic skyrmions in ultrathin magnetic nanostructures, Nature Nanotechnology 2016 11:5 **11**, 449 (2016).

[28] N. Romming, A. Kubetzka, C. Hanneken, K. Von Bergmann, and R. Wiesendanger, Field-Dependent Size and Shape of Single Magnetic Skyrmions, PRL **114**, 177203 (2015).

[29] X. S. Wang, H. Y. Yuan, and X. R. Wang, A theory on skyrmion size, Communications Physics **1**, 31 (2018).

[30] F. Büttner, I. Lemesh, and G. S. Beach, Theory of isolated magnetic skyrmions: From fundamentals to room temperature applications, Scientific Reports **8**, 1 (2018).

[31] E.Tremsina; G.Beach, Supplementary Material for Atomistic Simulations of Distortion-limited High-speed Dynamics of Antiferromagnetic Skyrmions , Physical Review B , 1 (2022).

[32] A. Bogdanovand A. Hubert, Thermodynamically stable magnetic vortex states in magnetic crystals, Journal of Magnetism and Magnetic Materials **138**, 255 (1994).

[33] P. F. Bessarab, D. Yudin, D. R. Gulevich, P. Wadley, M. Titov, and O. A. Tretiakov, Stability and lifetime of antiferromagnetic skyrmions, Physical Review B **99**, 140411 (2019).

[34] S. Rohartand A. Thiaville, Skyrmion confinement in ultrathin film nanostructures in the presence of Dzyaloshinskii-Moriya interaction, Physical Review B **88**, 184422 (2013).

[35] K.-W. Moon, B. S. Chun, W. Kim, Z. Q. Qiu, and C. Hwang, Control of skyrmion magnetic bubble gyration, Physical Review B **89**, 064413 (2014).

[36] L. Liu, W. Chen, and Y. Zheng, Current-Driven Skyrmion Motion Beyond Linear Regime: Interplay between Skyrmion Transport and Deformation, Physical Review Applied **10**, 24077 (2020).

[37] A. K. Zvezdin, V. I. Belotelov, and K. A. Zvezdin, Gyroscopic force acting on the magnetic vortex in a weak ferromagnet, JETP Letters 2008 87:7 **87**, 381 (2008).

[38] X. Zhang, Y. Zhou, and M. Ezawa, Antiferromagnetic Skyrmion: Stability, Creation and

Manipulation, Scientific Reports **6**, 24795 (2016).

[39] Y. Hirata, D. H. Kim, S. K. Kim, D. K. Lee, S. H. Oh, D. Y. Kim, T. Nishimura, T. Okuno, Y. Futakawa, H. Yoshikawa, A. Tsukamoto, Y. Tserkovnyak, Y. Shiota, T. Moriyama, S. B. Choe, K. J. Lee, and T. Ono, Vanishing skyrmion Hall effect at the angular momentum compensation temperature of a ferrimagnet, Nature Nanotechnology 2019 14:3 **14**, 232 (2019).

[40] L. Shen, X. Li, Y. Zhao, J. Xia, G. Zhao, and Y. Zhou, Current-Induced Dynamics of the Antiferromagnetic Skyrmion and Skyrmionium, Physical Review Applied **10**, 64033 (2019).

[41] M. W. Danielsand M. D. Stiles, A new spin on special relativity, Science **370**, 1413 (2021).

[42] R. F. L. Evans, W. J. Fan, P. Chureemart, T. A. Ostler, M. O. A. Ellis, and R. W. Chantrell, Atomistic spin model simulations of magnetic nanomaterials, Journal of Physics: Condensed Matter **26**, 103202 (2014).

[43] K. Litzius, J. Leliaert, P. Bassirian, D. Rodrigues, S. Kromin, I. Lemesh, J. Zazvorka, K. J. Lee, J. Mulkers, N. Kerber, D. Heinze, N. Keil, R. M. Reeve, M. Weigand, B. Van Waeyenberge, G. Schütz, K. Everschor-Sitte, G. S. Beach, and M. Kläui, The role of temperature and drive current in skyrmion dynamics, Nature Electronics **3**, 30 (2020).

[44] W. Jiang, X. Zhang, G. Yu, W. Zhang, X. Wang, M. Benjamin Jungfleisch, J. E. Pearson, X. Cheng, O. Heinonen, K. L. Wang, Y. Zhou, A. Hoffmann, and S. G. Te Velthuis, Direct observation of the skyrmion Hall effect, Nature Physics 2016 13:2 **13**, 162 (2016).

[45] B. A. Ivanov, E. G. Galkina, V. E. Kireev, N. E. Kulagin, R. V. Ovcharov, and R. S. Khymyn, Nonstationary forced motion of domain walls in ferrimagnets near the spin compensation point, Low Temperature Physics **46**, 841 (2020).

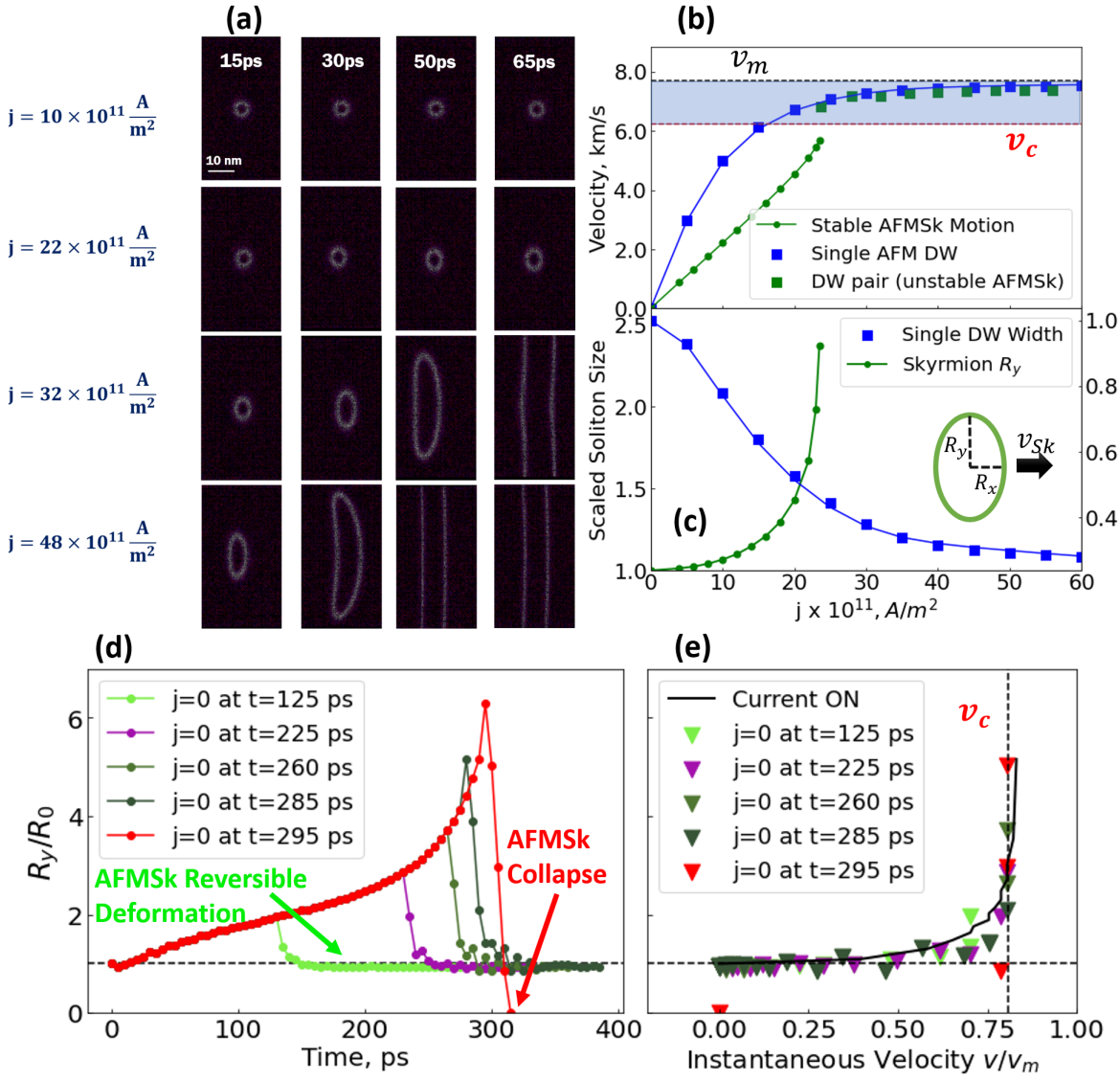

FIG. 1. (a)Intermediate magnetization profiles of travelling AFSMks, showing the varying degrees of dynamic elliptical deformation as the skyrmion is being accelerated from rest. (b) skyrmion vs single DW current-driven dynamics; DWs undergo relativistic velocity saturation, while skyrmions can only exhibit stable dynamics below a threshold v_c, which is linked to their elliptical deformation and eventual breakdown into a pair of DWs. (c)Dynamic changes in dimensions of travelling skyrmion and single DW. The skyrmion undergoes elliptical elongation - a large increase in transverse radius and a smaller increase in the parallel radius, while a single DW contracts following the Lorentz relationship. R_0 and Δ_0 are the equilibrium AFMSk radius and single DW width, respectively. (d)-(e) Reversibility of AFMSk dynamic deformation and critical collapsing behavior; plotted is the scaled transverse radius R_y versus (d)time and (e)fractional instantaneous velocity for various current pulse lengths; after a certain time $\tau = 300$ps (shown in red), the AFMSk can no longer return to its equilibrium state.

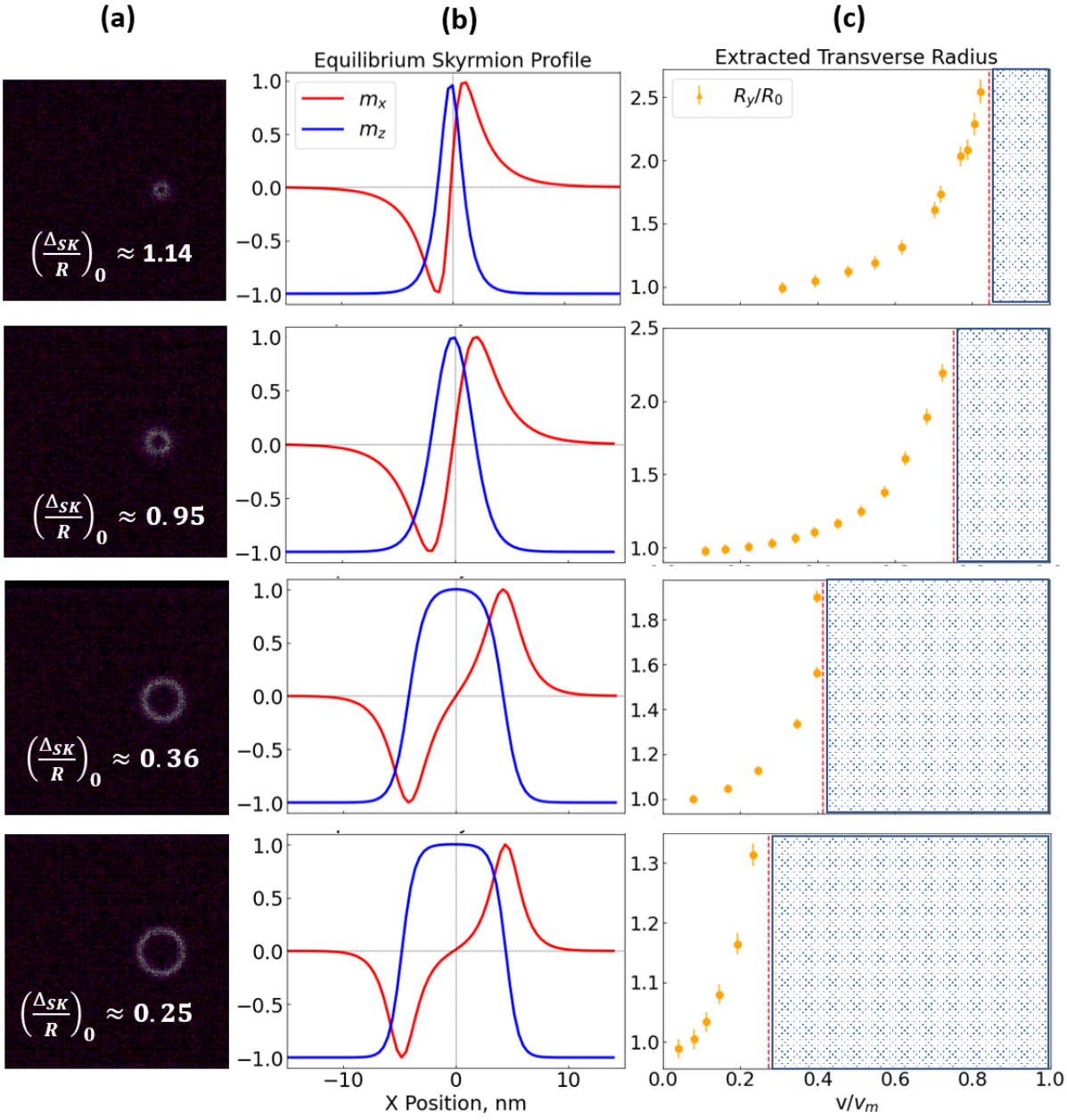

FIG. 2. Dynamic changes in AFMSk dimensions versus fractional velocity for AFM skyrmions of various compactness. (a)-(b) Equilibrium AFMSk profiles: (a) two-dimensional plot, (b) magnetization through the horizontal central axis with zero-centered X coordinates. (c) extracted transverse AFMSk radius R_y, as a function of the normalized velocity, showing the onset of critical expansion occurring at lower velocities for less compact AFMSks.

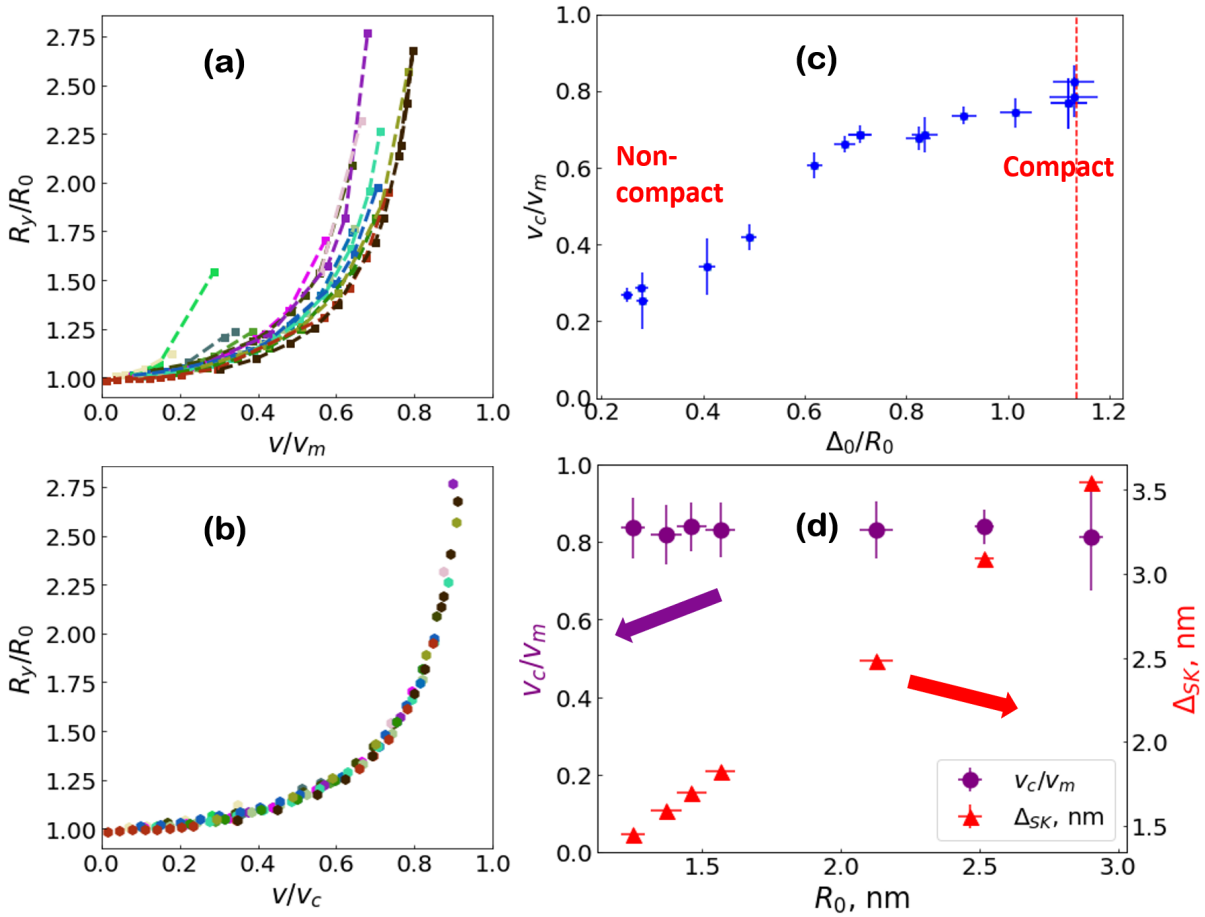

FIG. 3. Dynamic deformation analysis for AFMSks of various material parameters and equilibrium dimensions, given by Table S1 in the Supplementary Material[31]. (a)-(b) Vertical radial deformation R_y versus velocity normalized by (a)v_m, (b)v_c. (c) extracted critical velocity versus skyrmion compactness ratio. The red dashed line represents the theoretical limit of skyrmion compactness. d) (Red) - extracted critical velocity for AFMSks of equal compactness values but different physical dimensions; (purple) - extracted values of $\frac{v_c}{v_m}$ are unchanged as the dimensional parameters are varied.

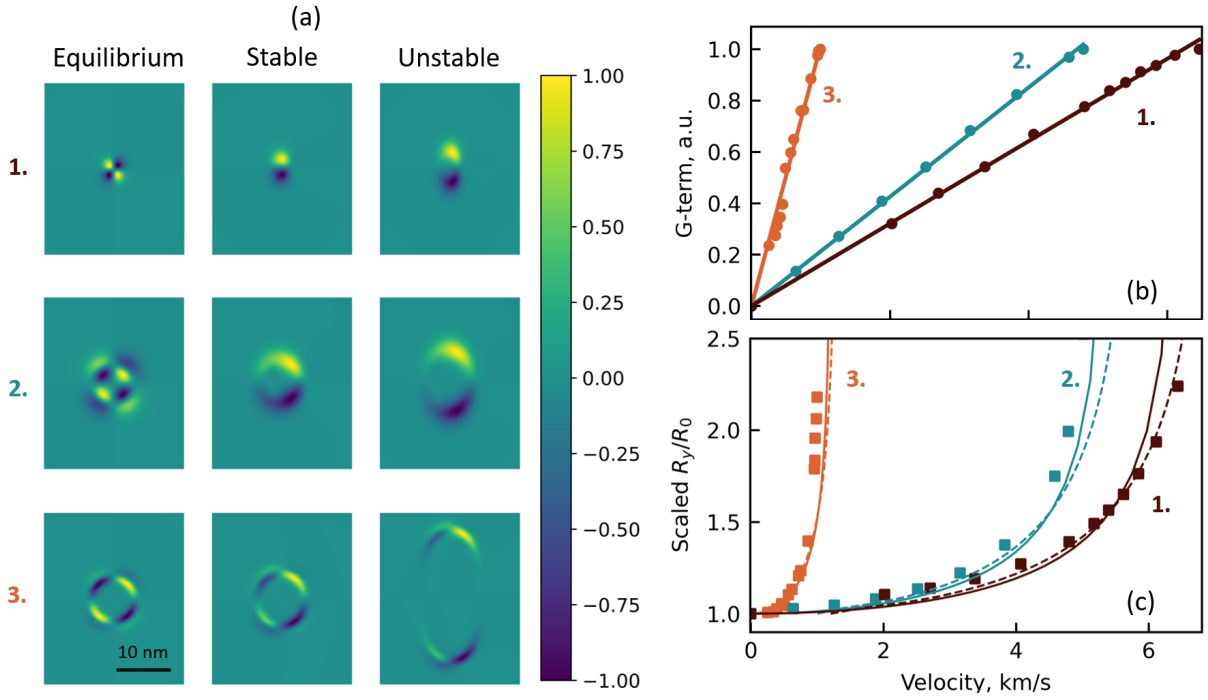

FIG. 4. (a) Two-dimensional plots of the total gyrotropic force term, showing the presence of local imbalanced gyrotropic forces acting on the two antiferromagnetic sublattices, when the AFMSk is in motion. AFMSks of three different compactness values are considered in panels 1-3. The equilibrium (leftmost) images show a perfect cancellation of the forces around the skyrmion perimeter, however, when in motion, a top-bottom asymmetry is apparent. (b) Differential gyrotropic force, computed as the difference of forces acting on the top/bottom half-skyrmions. A linear increase with velocity is observed for all three cases. (c) Scaled transverse radius R_y versus velocity. The numerical data (shown in square markers) are compared with curves derived from the elastic force model, and approximating the elliptical skyrmion energy. The dashed curve uses numerical values of R_y, computing the energy derivative, while the solid line uses numerical data for velocity, solving for the radius R_y.

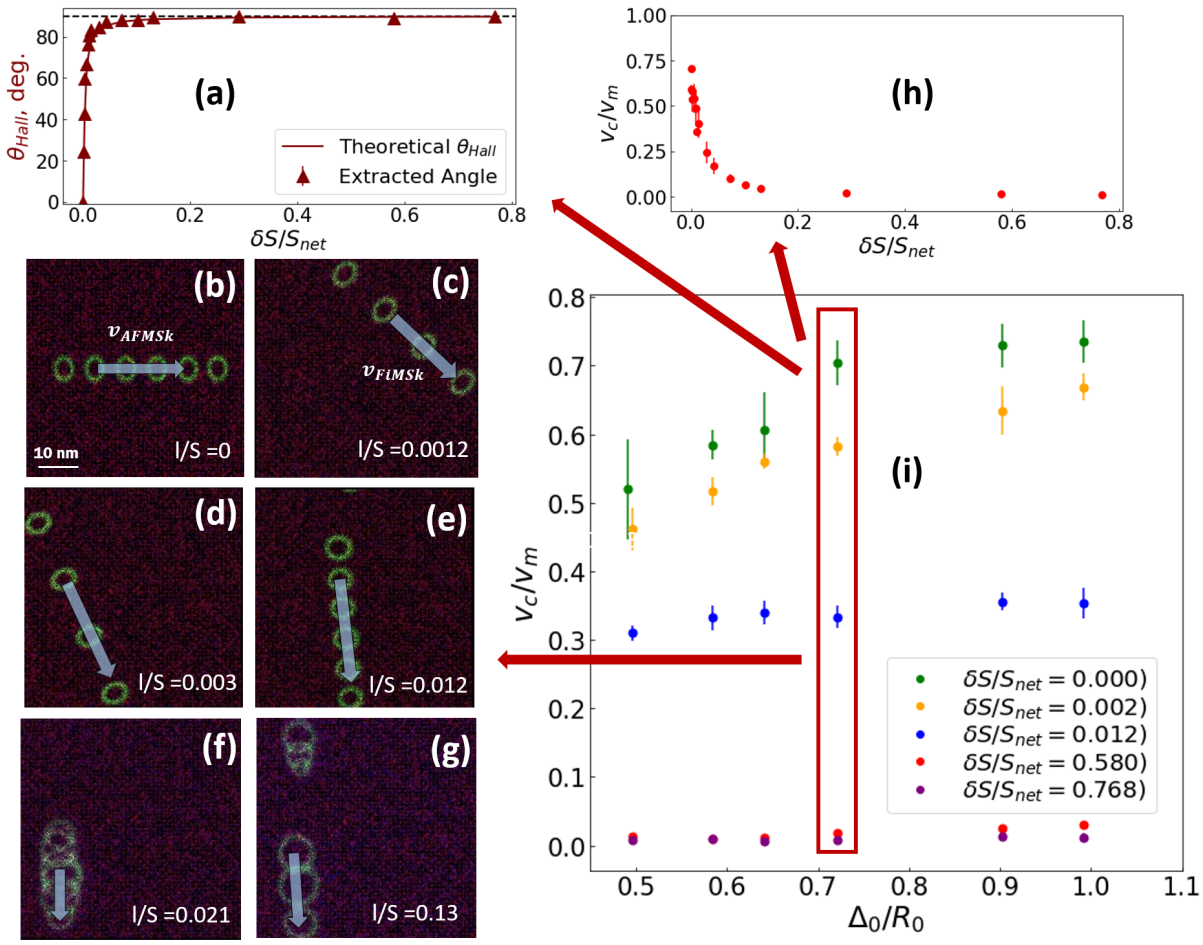

FIG. 5. Dynamics of FiM skyrmions of varying net angular momentum values. S_{net} is maintained constant, while toggling δS and capturing FiMSk dynamics. (a) Theoretical values (using Eq.22 with equilibrium FiMSk dimensions), and numerical results for Skyrmion Hall angle versus scaled angular momentum, $\delta S/S_{net}$. (b)-(g) 2D panels of FiMSk travelling near critical velocity, showing deformation effects. (h) extracted critical velocity drop-off as a function of angular momentum. (i) sweep over FiMSk of various compactness values, showing critical velocity correlation

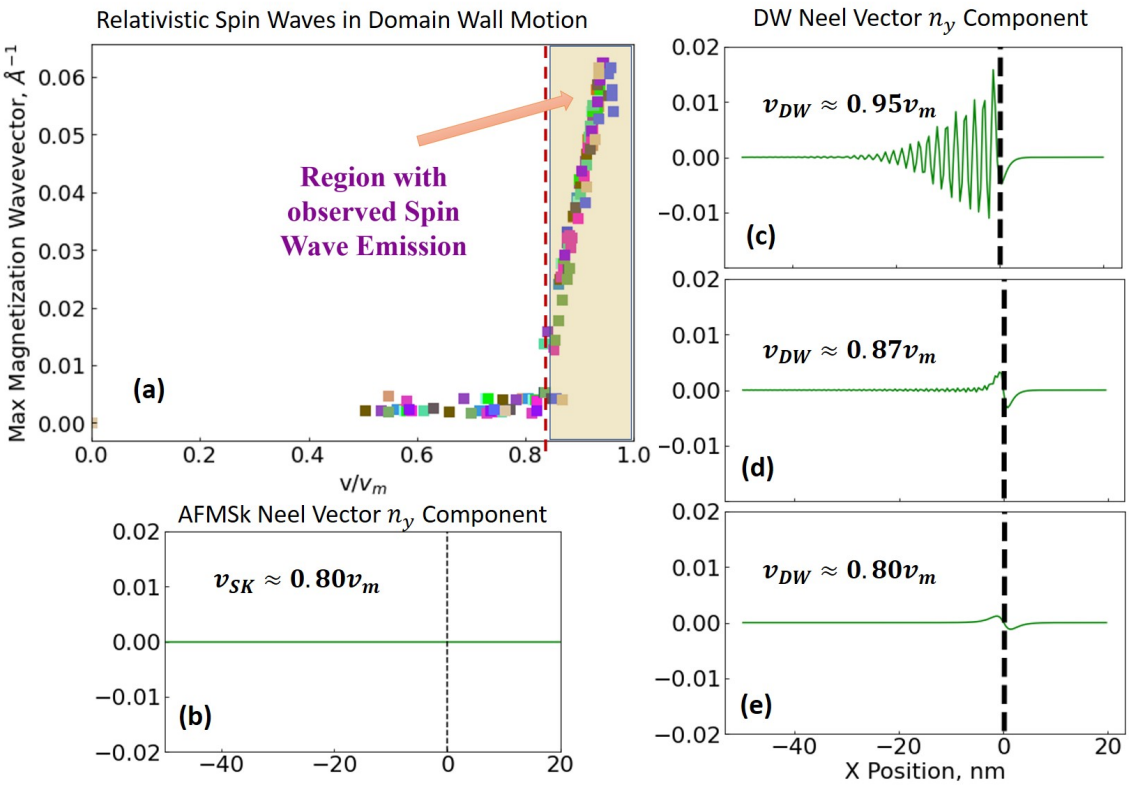

FIG. 6. Characterization of Spin Wave Emissions (SWE) using the maximum component wavevector from the Fourier transform of the Neel vector n_y profile of a travelling single AFM DW as a function of its relative velocity. It is shown that the onset of SWE occurs at approximately the same point as the maximum reachable AFMSk velocity, dictated by the v_c of a skyrmion of maximum compactness.The parameters chosen are the same as in Fig.3. (b)-(d) Spatial plot of the n_y component of the Neel vector from a soliton travelling to the right under SOT: (b)AFMSk and (c)-(e)DW. The high-frequency oscillations observed in panels (c)-(d) are consistent with previously observed high-velocity relativistic SWE and are not observed for travelling AFMSk.